International Journal of Concrete Structures and Materials

RESEARCH

Open Access

Shear Strengthening of High-Strength Reinforced Concrete Deep Beams with Openings Using High-Performance Concrete Mortars

Ahmed Hamoda[1*], Mohamed Emara[2], Mizan Ahmed[3] and Aref A. Abadel[4]

Abstract

Reinforced concrete (RC) deep beams often necessitate openings in their web to facilitate building utilities. These openings compromise the shear resistance of the beams and, therefore, should be strengthened in their critical shear zone. This study proposes externally bonded high-performance concrete (HPC) mortars layers strengthened with steel wire mesh to strengthen the shear capacity of high-strength RC deep beams with openings within their shear span. To facilitate this, an experimental program consisting of testing ten high-strength RC deep beams was carried out. The test parameters include the effects of opening, types of HPC mortars, namely, engineered cementitious composites (ECC) and ultra-high-performance fiber-reinforced concrete (UHFRC) mortars, the configuration of the opening (circular, square), and the size of the openings. Two strengthened beams were fabricated without openings, while the remaining incorporated various opening configurations. The results demonstrated the shear performance of the beams increases using the proposed strengthening technique. The increases in ultimate load capacity ranged from 5 to 68%, elastic stiffness improved between 8 and 97%, and energy absorption capacity enhanced from 7 to 127%. Increasing the opening size reduces the strength, stiffness, and energy absorption capacity of the beam. Furthermore, beams with circular openings exhibited better performance than their square counterparts. The specific design and strengthening strategies employed effectively improve their load-bearing capacity concerning the opening size ratio. Application of the HPC mortars with higher compressive and tensile strength further results in the improvement of their shear performance. In addition, a finite element model (FEM) was developed to simulate the performance of tested beams and compare the accuracy of the FEM against the test results. It was found that the adaptation of the Concrete Damage Plasticity (CDP) model with the parameters adopted in this study can accurately predict the behavior of the tested beams. An average error of only 4% was obtained for the experiment-to-predicted load for cracking and ultimate load. Furthermore, based on the parametric study performed on beams with circular openings strengthened with ECC layers, it is proposed that for practical design purposes the thickness of the ECC layer to the thickness of the beam (t_{ECCC}/t_{beam}) ratio should not exceed 0.32.

Keywords Deep beams, High, Strength, Engineered cementitious composites, Ultra, High, Performance fiber, Reinforced concrete, Openings, Strengthening, Shear capacity

Journal information: ISSN 1976-0485 / eISSN 2234-1315.

*Correspondence:
Ahmed Hamoda
ahmed_hamoda@eng.kfs.edu.eg
Full list of author information is available at the end of the article

1 Introduction

High-strength reinforced concrete (RC) deep beams have grown in popularity across various structural engineering applications including the construction of bridges, and high-rise buildings, due to their superior shear resistance (Choi et al., 2012). This enhanced resistance can be attributed to the increased depth-to-span ratio. Their deeper profile facilitates the transfer of shear forces through an internal arching action within the beam itself (Hamoda et al., 2024d, f; Nakamura et al., 2018; Shakir & Alghazali, 2024).

Deep beams possess disturbed regions (D-region), where significant disturbance of contour lines of the flexural stresses exists which results in stress concentration at D-regions (Shakir & Hannon, 2024; Shakir & Hanoon, 2023) . Furthermore, deep beams often require openings to accommodate essential utilities like electrical lines, communication systems, and mechanical installations. However, these openings induced D-region, disrupt the flow of stress within this region (Shakir & Hamad, 2023; Shakir et al., 2023). This disruption can lead to a reduction in the overall shear capacity, potentially compromising the structural integrity (Al-Mahbashi et al., 2023; Ghali et al., 2021; Jasim et al., 2020; Kachouh et al., 2022; Shyamala, 2022). Therefore, strengthening may be necessitated to guarantee its structural integrity. Researchers have explored various methods to enhance deep beam performance, including the application of fiber-reinforced polymers (FRP) (Abadel et al., 2022; Akkaya et al., 2022b, 2024; Ary & Kang, 2012; Osman et al., 2017; Xing et al., 2024), high-performance concrete (HPC) (Abadel et al., 2022; Al-Enezi et al., 2023), or steel plates (Chandrakanth & Kavitha, 2020; Farouk et al., 2023), and hybrid U-jackets composites (Cakir et al., 2023). These strengthening materials can be attached externally using bonding techniques or embedded near the concrete surface using a near-surface mounted (NSM) approach (Akkaya et al., 2022a; Al-khreisat et al., 2023; Elsayed et al., 2022; Fatehi Makki et al., 2019; Heydari et al., 2023; Kumari & Nayak, 2021; Li et al., 2022; Rahim et al., 2020; Yousef et al., 2018, 2023). Although the application of an externally bonded HPC layer to strengthen slender RC beams has been investigated earlier (Emara et al., 2023; Hamoda et al., 2024b; Koutas et al., 2019; Wang et al., 2019), studies on its use in strengthening deep beams are still limited.

Lee et al. (2011) studied the impact of carbon fiber-reinforced polymer (CFRP) sheet strengthening on the structural behavior of T-shaped RC deep beams lacking stirrups. The investigation revealed that several factors significantly influence the performance of such strengthened beams including the length of CFRP, fiber direction in CFRP sheets, and anchorage of CFRP sheets. Overall, horizontal fiber orientation by covering the full shear span was found to be the most beneficial. The increase of the ultimate load, elastic stiffness, and energy absorption for this particular configuration compared to the control beam was measured as about 66%, 41%, and 152%. Moreover, proper anchorage of the CFRP sheets is essential to ensure their effectiveness in strengthening the beam. El Maaddawy and Sherif (2009) also reported that FRP composites significantly improve the maximum capacity of deep beams with an increase ranging from 35 to 70%. Interestingly, the location of the openings within the beam also influenced the outcome. Beams with openings closer to the top benefitted the most in terms of shear resistance, while FRP strengthening proved more effective for improving stiffness when the openings were positioned in the middle of the web. These findings suggest that the placement of openings and the specific goal (increased shear capacity or stiffness) can influence the optimal location for FRP strengthening. Dutta et al. (2022) explored the effectiveness of externally bonded glass fiber-reinforced polymer (GFRP) fabrics in strengthening the structural behavior of RC deep beams subjected to shear stress. The maximum load of the beams increased by 108%. In addition, it was reported that with more than 3 layers of GFRP sheets, the shear strength, absorb energy, and stiffness of the beams decreased. Arabzadeh and Karimizadeh (2019) explored the use of externally bonded FRP composites to improve the shear performance of deep beams with circular openings. It was reported that using FRP improved the ultimate load of the tested beams by 68%.

Chandrakanth and Kavitha (2020) explored an innovative approach to strengthen RC deep beams by substituting traditional stirrups with steel plates. Interestingly, their findings revealed that solid steel plates decreased the load capacity. However, perforated plates with strategically placed holes offered a promising alternative. These perforations enhanced the bonding between the steel and concrete, ultimately leading to a significant increase in load capacity. Their study identified a configuration with eight circular holes, each 50 mm in diameter, as the most effective design. A study by Farouk et al. (2023) demonstrated that externally bonded steel plates significantly enhance the performance of concrete deep beams with openings. These plates promote a more uniform distribution of cracks across the beam, delaying failure and extending its lifespan. The benefits were even more pronounced when the steel plates were combined with external anchors. The combined effect resulted in a substantial improvement in the shear capacity of the beams. Recently, Hamoda et al. (2024d) examined the effectiveness of using glass fiber mesh with strain-hardening cementitious materials in strengthening deep beams without openings. It was found that the proposed

method increased the ultimate load of the deep beams by up to 82%, cracking load by up to 73%, elastic stiffness by up to 457%, and energy absorption by up to 380% compared to the unstrengthened control beam. Recently, T-deep beams with deficient shear reinforcement having a large opening within the shear spans were strengthened using the stitching method employing the near-surface mounted steel bars and externally bonded carbon fibers reinforced polymers technique (Shakir & Yahya, 2024). It was found that stitching by externally bonded carbon sheets resulted in the improvement of the capacity of 96% at the top location compared to the control beam.

While prior research has investigated strengthening deep beams with or without openings using FRP composites, the poor performance of FRP composites on fire hinders their wider adaptation in real life. This study proposes externally bonded HPC layers strengthened with steel wire mesh to strengthen the shear-deficient high-strength RC deep beams with or without openings within their shear span. However, there has been no study carried out to explore the structural performance of RC deep beams strengthened with bonded HPC layers, namely, engineered cementitious composites (ECC) and ultra-high-performance fiber-reinforced concrete (UHFRC) reinforced with steel wire mesh. The effects of the presence of opening, shape, and size of openings on the structural performance of deep beams strengthened using ECC or UHFRC layer. Finite element models (FEM) were also developed to analyze the performance of such beams.

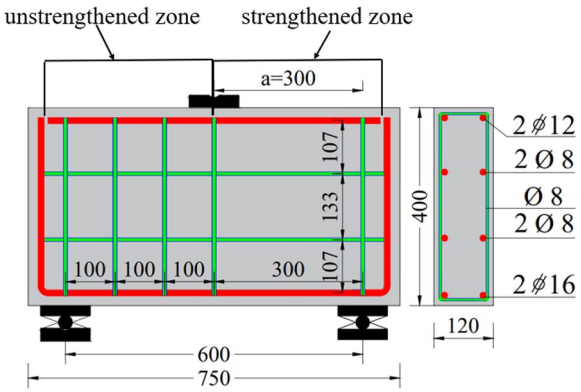

Fig. 1 Dimensions and reinforcement of tested deep beams. (Units: mm)

Table 1 Details of the test specimens

Group	Specimen's ID	Concrete type	Opening type	Opening size
G1	B0	Unstrengthened	–	–
G2	B-ECC		–	–
	B-E-C1	ECC	Circular	D = 85 mm
	B-E-S1		Square	L = 85 mm
	B-E-S2		Square	L = 110 mm
G3	B-UHFRC		–	–
	B-U-C1	UHFRC	Circular	D = 85 mm
	B-U-C2		Circular	D = 110 mm
	B-U-S1		Square	L = 85 mm
	B-U-S2		Square	L = 110 mm

2 Testing Program

2.1 Details of the Test Specimen

Ten rectangular high-strength RC deep beams were cast and tested under a three-point loading configuration for this study. All beams shared identical dimensions of 120 × 400 × 750 mm (width × depth × overall length), with a 600 mm distance between supports, as illustrated in Fig. 1. For main reinforcement, all beams included two 16 mm diameter U-shaped steel bars at the bottom and two 12 mm diameter steel bars at the top. The provided longitudinal reinforcement was selected to prevent flexural cracking. In addition, each beam incorporated four 8 mm diameter side steel bars, two on each side. To provide shear resistance, stirrups made from 8 mm diameter steel were spaced at 100 mm intervals along half the length of each beam. To assess the effectiveness of the proposed strengthening configuration in improving shear resistance, stirrups were strategically omitted from half of each beam. This approach allows for a clear evaluation of how the strengthening elements enhance the beams' ability to resist shear forces.

The specimens were divided into three groups of as shown in Table 1. Group G1 consisted of the control beam B0 which was un-strengthened. The second (G2) and third group (G3) focused on the influence of different concrete tpes on the beams with and without opening shape. For the beams with openings, the shapes (circular or square) and size of the openings are examined (see Fig. 2). In groups G2, and G3, one solid beam, namely, B-ECC, and B-UHFRC, were also examined. Both groups used welded steel mesh (WSM) to reinforce the strengthening layers, which were anchored to the beam surface using steel bolts, as shown in Fig. 2. In naming the specimens, B0 refers to control sample, B-ECC and B-UHFRC representing solid beams with ECC and UHFRC, respectively. For samples with openings, the letters (E and U) followed by 'B' represent ECC and UHFRC. The letter 'C' or 'S' stands for circular or square openings. The number '1' or '2' represents different opening sizes. The locations of the openings are shown in Fig. 2. Reinforcement around the openings were cut to facilititate formwork.

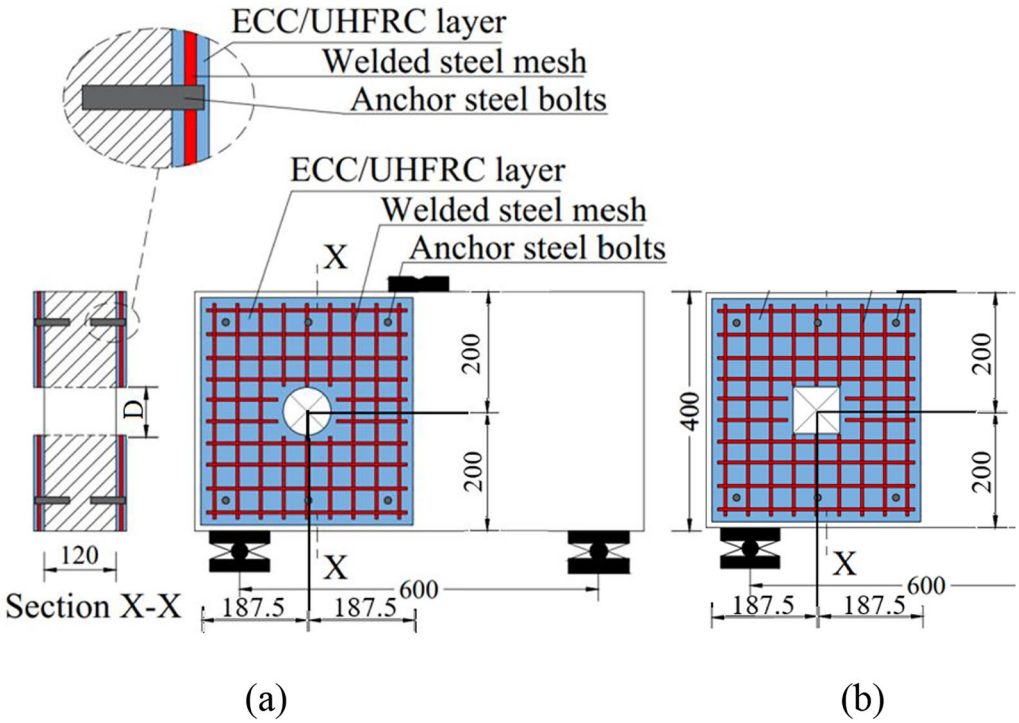

Fig. 2 Schematic of strengthening configurations: **a** beams with circular opening and **b** beams with square opening. (Units in mm)

2.2 Material Properties and Mix Proportion

All beams were cast from ready-mix high-strength concrete (HSC) before strengthening prior to strengthening in the specific zone. Upon casting, all the samples were cured in an identical condition. During the curing before and after the strengthening process, plastic sheeting prevents moisture loss and facilitates proper curing. The concrete compressive strength was measured using 150 × 300 mm cylinders recommended by ACI 318-19 (2019) and tested using the recommendation given by ASTM C469 (2022). The uniaxial tensile performance of concrete was measured by testing dog-bone-shaped specimens according to ASTM C1583 (2020). To characterize the material properties, cylindrical specimens with a dimension of 150 mm × 300 mm, and dogbone-shaped specimens were tested in determining compressive and tensile strengths for all concretes. The compressive and tensile strength of HSC was 93 and 4.35 MPa, respectively. ECC and UHFRC were used for strengthening purposes. Table 2 details the mix proportions of ECC and UHFRC used in the experiment. The Polypropylene fiber (PP) fibers used in this study had a density of 0.91 (g/cm^3), diameter of 32 µm, length of 12 mm, tensile strength of 467–584 MPa, and a modulus of elasticity of 3.5–6 GPa according to the supplier ("Sika Egypt Group 2021"). The mechanical properties of ECC and UHFRC are presented in Table 2, along with the experimental and idealized stress–strain responses illustrated in Fig. 3. In addition, tensile coupon tests on reinforcing steels, WSM, and steel bolts were carried out to determine their mechanical characteristics, tested according to A370-10 (2006). The WSM had an opening size of (40 × 40) mm^2 with a bar diameter of

Table 2 Mix proportions and properties of ECC and UHFRC mortars

Concrete	Cement (kg/m^3)	Fine aggregate (kg/m^3)	Fly ash (kg/m^3)	Silica fume (kg/m^3)	Water to bender ratio	Polypropylene fiber (%)	High-range water reducer (kg/m^3)	Compressive strength f_c (N/mm^2)	Tensile strength f_t (N/mm^2)
HSC (premix)	–	–	–	–	–	–	–	93	4.35
UHFRC	850	1030	–	200	0.20	2	28	127	6.7
ECC	558	436	665	–	0.23	2	15	52	4.43

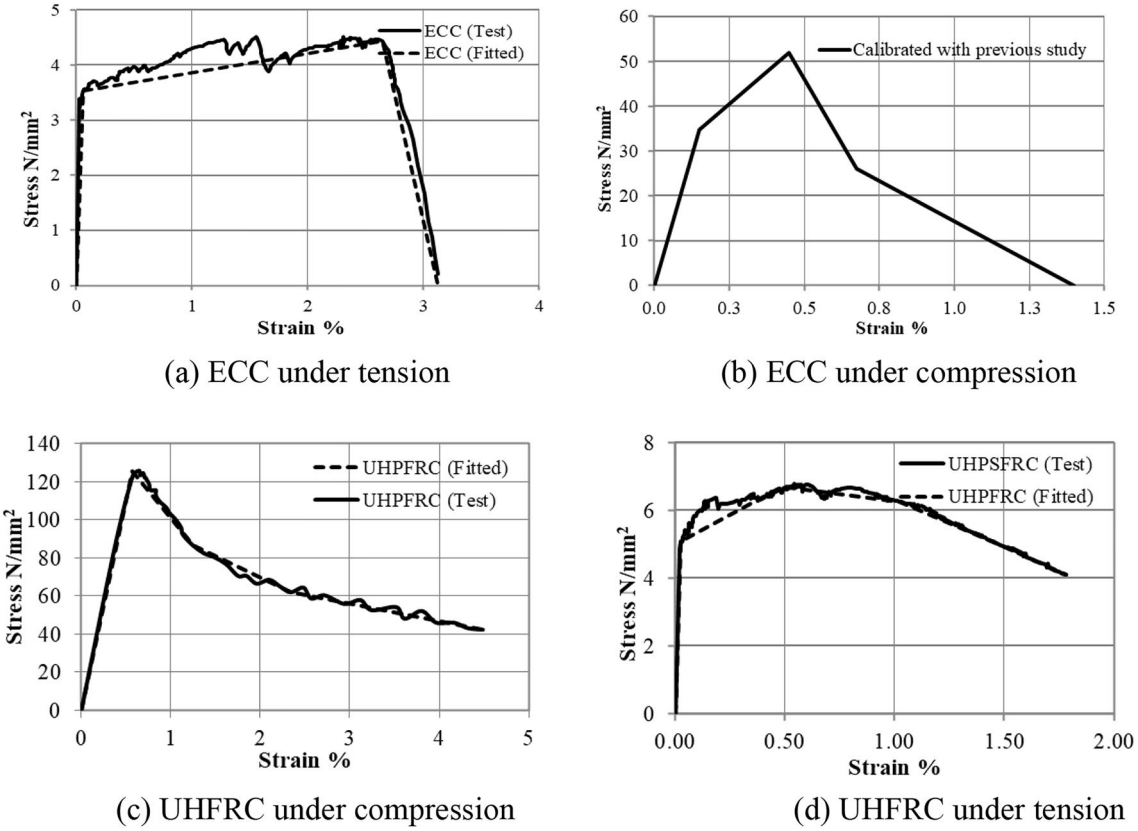

Fig. 3 Stress–strain curves of ECC and UHFRC

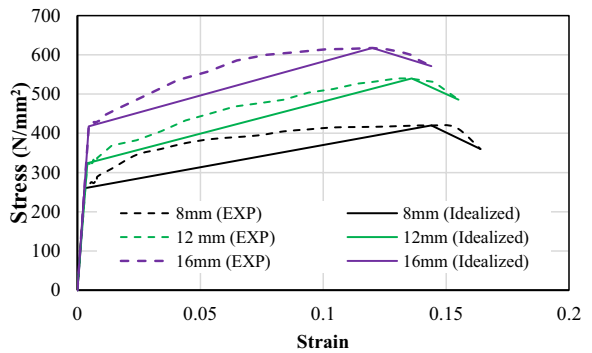

Fig. 4 Measured and idealized stress–strain curves for steel elements

3 mm, as shown in Fig. 5c. Steel bolts with a diameter of 12 mm and length of 150 mm across the beam width to cover both strengthening layers, as shown in Fig. 5b. The tensile results presented in Fig. 4 were averaged from the tests of three coupons. The observed experimental and idealized stress–strain responses for the steel are given in Fig. 4. Table 3 presents the yield and tensile strength of all steel elements.

Table 3 Material properties of steel elements

Steel element	Yield strength (MPa)	Tensile strength (MPa)
8 mm	267	441
12 mm	364	529
16 mm	417	602
Bolt	382	423
WSM	275	355

2.3 Specimens' Preparation

Initially, tested beams were cast prior to the strengthening process taking place after 28 days of their curing. To strengthen the beam, a multi-step process was implemented (see Fig. 5). The strengthening process of the tested specimens includes roughening of the beam surface to improve the adhesion between the beam and the strengthening layer. Anchor bolts were used to avoid premature interface failure. The WSM was then positioned on the designated shear zones on both sides of the beams followed by the application of the ECC/

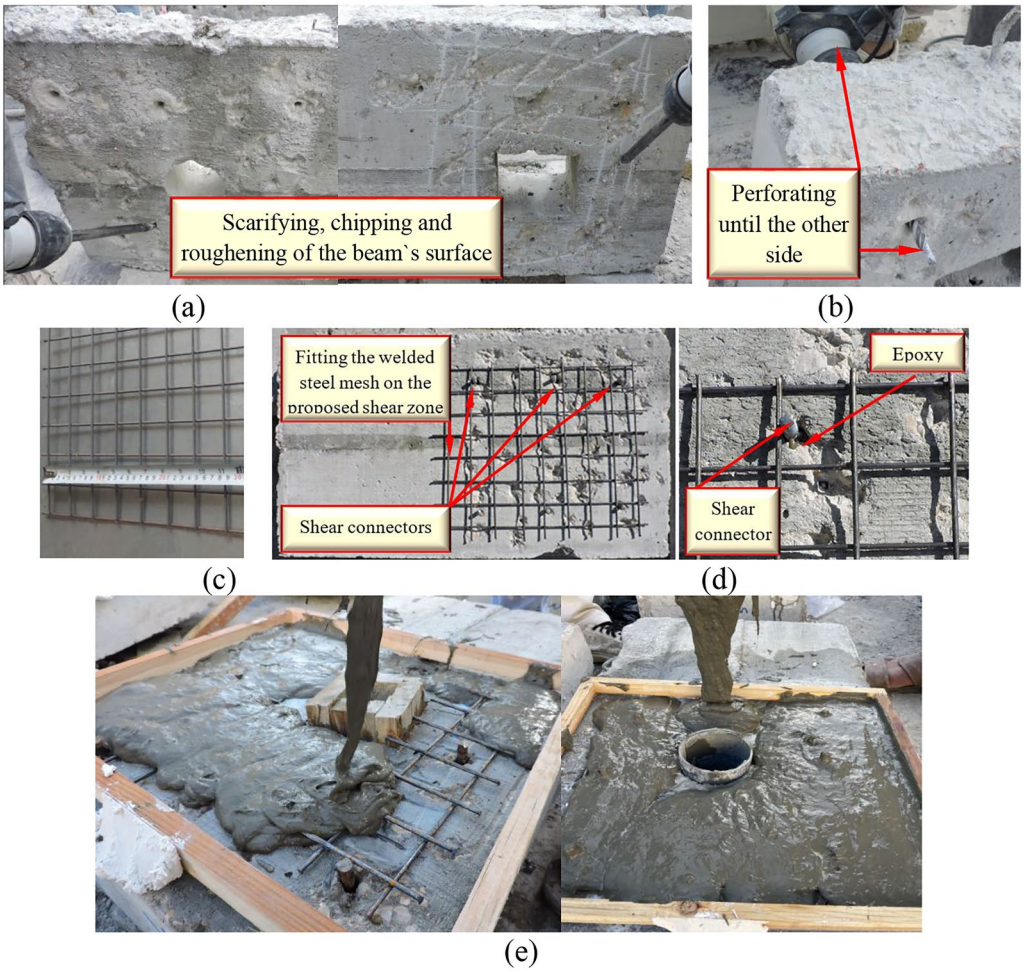

Fig. 5 Strengthening process: **a** surface roughening, **b** perforation, **c** welded steel mesh used herein, **d** installation of WSM, **e** casting HPC

UHFRC layer with a thickness of 10 mm. The beams were left for 28 days to cure before the testing.

2.4 Testing Setup and Instrumentation

Fig. 6 depicts the experimental setup employing a three-point bending test. The proposed shear-strengthened zone of the beams strengthened with ECC and UHFRC was painted in green and blue, respectively, for better visualization. The tested beams were rested on two hinged supports spaced 600 mm apart. The steel plates were 100 × 150 mm with a thickness of 20 mm. To ensure consistent loading, a displacement-controlled regime applies the load at a rate of 6 mm/min. The load was transferred by steel I-column. A Linear Variable Differential Transformer (LVDT) positioned at the beam's bottom surface, as shown in Fig. 6, measured the mid-span deflection throughout the test. Two PI-shape displacement transducers were used to measure the width of the shear cracks. Cracks were marked as appearing during the applied load until the failure.

3 Test Observations

3.1 Failure Patterns

The control beam (B0) displayed a classic shear failure (see Fig. 7) in the zone without shear reinforcement. Cracks formed diagonally along the weakened shear span near the support, accompanied by crushing concrete. The first crack appeared at 36% of the ultimate load (see Table 4) and was initiated near the support within the weakened zone. As the load increased, this initial crack propagated diagonally toward the loading point, with additional cracks forming and growing. At the failure, the beam suffered a brittle sudden failure in the concrete compressive strut, specifically in the diagonal area linking the loading and support points. This type of failure underscored the absence of shear stirrups, which are generally employed to prevent such diagonal cracking.

Both ECC and UHFRC layers effectively delayed crack initiation in the strengthened beams (B-ECC and B-UHFRC, respectively). ECC delayed the initial cracking load by 6%, while UHFRC provided a more substantial

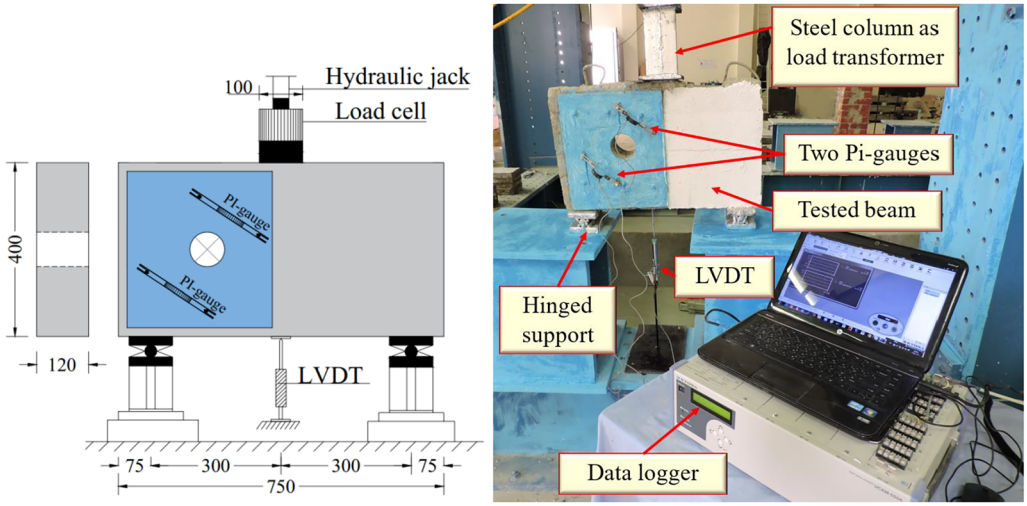

Fig. 6 Testing setup of the beams: **a** schematic drawing and **b** actual settings. (Units in mm)

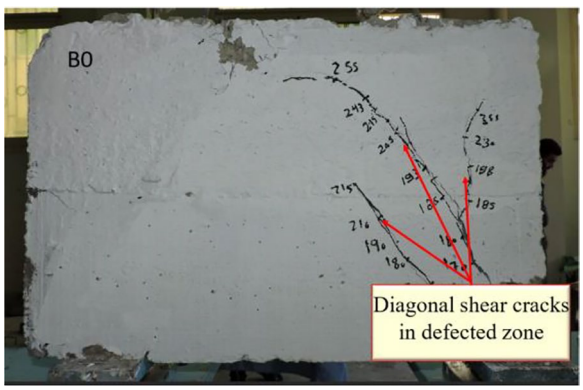

Fig. 7 Failure pattern of the beam B0

delay of 32% according to Table 4. The crack patterns differed between the two beams. For beam B-ECC, initial cracks started near the support and progressed diagonally before the beam ultimately failed due to rupture of the ECC layer itself (see Fig. 8a). In contrast, B-UHFRC exhibited initial cracks at the support similar to B-ECC, but these cracks then propagated vertically before transitioning diagonally. Importantly, for both beams, cracks were primarily confined to the strengthened zone at lower loads. However, at higher loads, some limited cracking appeared in the non-strengthened zone of the UHFRC beam (see Fig. 8b). The enhanced performance of both ECC and UHFRC can be attributed to their exceptional elastic properties, which enable high tensile

Table 4 Summary of results of the tested beams

Specimen's ID	Cracking stage			Ultimate Stage			Elastic Stiffness, K (kN/mm)	K_B/K_{B0}	Absorbed Energy, E (kN. mm)	E_B/E_{B0}	*Failure mode
	P_{cr} (kN)	P_{crB}/P_{crB0}	Δ_{cr} (mm)	P_u (kN)	P_{uB}/P_{UB0}	Δ_{Pu} (mm)					
B0	160	1.00	0.94	280.35	1.00	4.45	108.67	1.00	1055.93	1.00	S
B-ECC	108.75	0.68	0.74	400.23	1.43	5.00	146.96	1.35	1812.50	1.72	(S + B) at Strn
B-E-C1	103.30	0.65	0.88	353.97	1.26	4.50	117.39	1.08	1754.64	1.66	S at Strn
B-E-S1	102.20	0.64	0.79	336.77	1.20	4.25	129.37	1.19	1302.71	1.23	S at Strn
B-E-S2	100.05	0.63	0.84	295.31	1.05	3.93	119.11	1.10	1164.97	1.10	S at Strn
B-UHFRC	134.67	0.84	0.63	470.12	1.68	6.06	213.76	1.97	2396.53	2.27	S at Strn
B-U-C1	130.55	0.82	0.73	425.01	1.52	4.70	178.84	1.65	1765.36	1.67	S at Un
B-U-C2	121.43	0.76	0.81	386.25	1.38	4.75	149.91	1.38	1458.85	1.38	S at Strn
B-U-S1	114.33	0.71	0.96	341.11	1.22	4.26	119.09	1.10	1132.37	1.07	S at Strn
B-U-S2	104.20	0.65	0.97	325.16	1.16	4.37	107.42	0.99	933.93	0.88	S at Strn

P_{cr}, Load corresponding to the first crack appeared; Δ_{cr}, Vertical deflection corresponding to P_{cr}; P_u, Ultimate load; Δ_{Pu}, Vertical deflection corresponding to P_u; E, Absorbed energy; K, elastic index

* Failure mode: S: Shear failure mode, B: bearing at the loading zone, Strn.: Strengthened zone, and Un.: unstrengthened zone

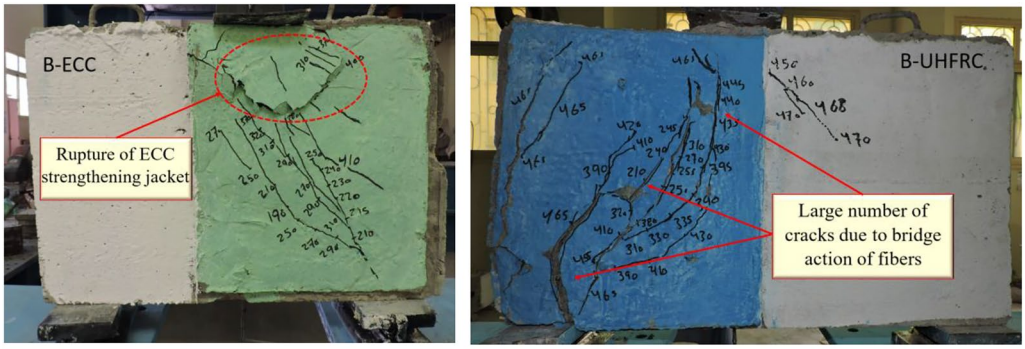

Fig. 8 Failure patterns of beams: **a** B-ECC and **b** B-UHFRC. (Note: green and blue painted sections are strengthened)

ductility and precise crack width control. In addition, the fibers within these materials effectively bridge cracks and distribute stress uniformly, preventing the development of large cracks and ensuring consistent performance under load.

For beams, with openings, strengthened using an ECC layer (Group G2), the failure modes are shown in Fig. 9. For the beam with a circular opening, cracks initiated near the top and bottom of the opening's diameter and propagated towards the supporting and loading points (see Fig. 9a). For the beams with square openings, cracks started at the corners (see Fig. 9b, c) and spread towards the bearing and loading regions. The first cracks appeared at about 29%, 30%, and 34% of the ultimate load for beams B-E-C1, B-E-S1, and B-E-S2, respectively. In the case of the beams with square openings, additional diagonal cracks formed due to stress concentrations at the corners, propagating between the edges of the plates and the opening. For the beams with a circular opening, under increased loading, cracks initiated at the mid-shear span and followed the curved contour of the opening in the strut direction. Ultimately, all beams in Group G2 exhibited cracks within the inner surface of the opening and failed due to the splitting of the strut within the strengthening layer, as illustrated in Fig. 9. However, this may be attributed to the superior crack-controlling performance of both ECC and UHFRC. The crack patterns displayed by these materials showed several hairline cracks, in contrast to the fewer, larger cracks typically seen in ordinary concrete types.

The failure pattern of beams in group G3 is shown in Fig. 10. Beam B-U-C1, featuring a circular opening and a UHFRC layer in the compromised shear zone, exhibited a improved failure pattern compared to other groups. Due to the smaller openings, the stress distribution of the strengthened region was higher than the non-strengthned side (white painted) which resulted in the failure in the non-strengthned zone of the beam. No cracks were detected in the strengthened zone, while a single major shear crack appeared at the support in the unstrengthened zone. This crack initiated around 30% of the ultimate load and propagated diagonally towards the loading point with increasing load, ultimately leading to a pure shear failure (see Fig. 10a) at the beam's full capacity. Beam B-U-C2, similar to B-U-C1 but with a larger opening, displayed a different cracking pattern. Cracks initiated around the lower half of the circular opening's perimeter and propagated towards the support (see Fig. 10b). In addition, more cracks appeared along the opening's inner surface, and two diagonal cracks were observed at the top of the strengthening layer. This may indicate that a larger opening may diminish the effectiveness of the UHFRC layer in preventing crack initiation.

For beams with square openings, strengthened with a UHFRC layer (B-U-S1 and B-U-S2), the location and direction of crack initiation depended on the opening size. In beams with smaller square openings, cracks started at the corner zone and propagated diagonally towards the loading and supporting points (see Fig. 10c). However, in beams with larger openings, cracks appeared and grew only in the region directly above the opening (see Fig. 10d). This indicates that the size of the opening impacts the stress distribution within the UHFRC layer, thereby influencing the initiation and propagation of cracks.

3.2 Load–Deflection Relationships

Fig. 11 illustrates the load–deflection curves, while the key results are presented in Table 4. As shown in Fig. 11, the control beam exhibited a linear behavior up to its first crack at a load of 102.15 kN, which is roughly 36% of its ultimate capacity. This mid-span deflection

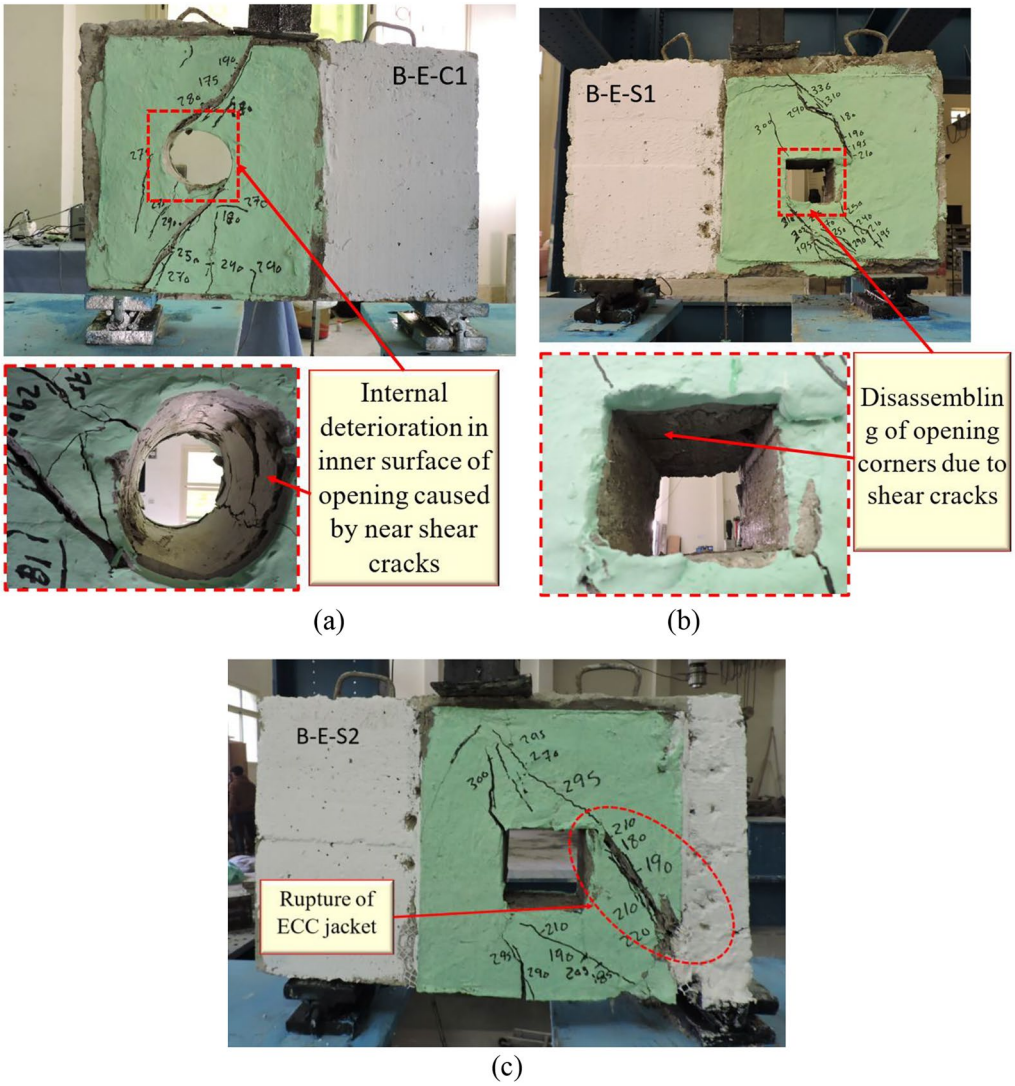

Fig. 9 Failure patterns of beams: **a** B-E-C1, **b** B-E-S1, and **c** Bem B-E-S2

corresponding to the first cracking load was approximately 0.94 mm. Beyond this point, the beam's stiffness began to decrease with increasing load until reaching around 250 kN. A more significant decline in stiffness occurred after this point. Ultimately, the control beam failed at a load of 280.35 kN, with a corresponding deflection of about 4.55 mm. Compared to the B0, both B–ECC and B–UHFRC beams in Group G1 exhibited similar overall behavior but with significantly improved performance (see Fig. 11a). They displayed higher cracking loads (increases of 6% and 32%, respectively) and lower mid-span deflections at these loads. Ultimately, these strengthened beams demonstrated remarkable load-carrying capacity, exceeding the control beam by 43% (B-ECC) and 68% (B-UHFRC) at failure. These findings clearly illustrate the effectiveness of the strengthening techniques, with UHFRC providing a more significant enhancement compared to the ECC layer. The reason can be attributed to the higher compressive and tensile strength of the UHFRC concrete compared to ECC.

Beam B-E-C1 in group G2, featuring a circular opening, exhibited a notable enhancement in overall performance compared to the control beam (see Table 4, Fig. 11b). While the initial cracking load only increased by 1%, the benefits became more pronounced beyond cracking point. Among beams with openings in the same group, those with circular openings exhibited superior performance compared to square openings (see Fig. 11b).

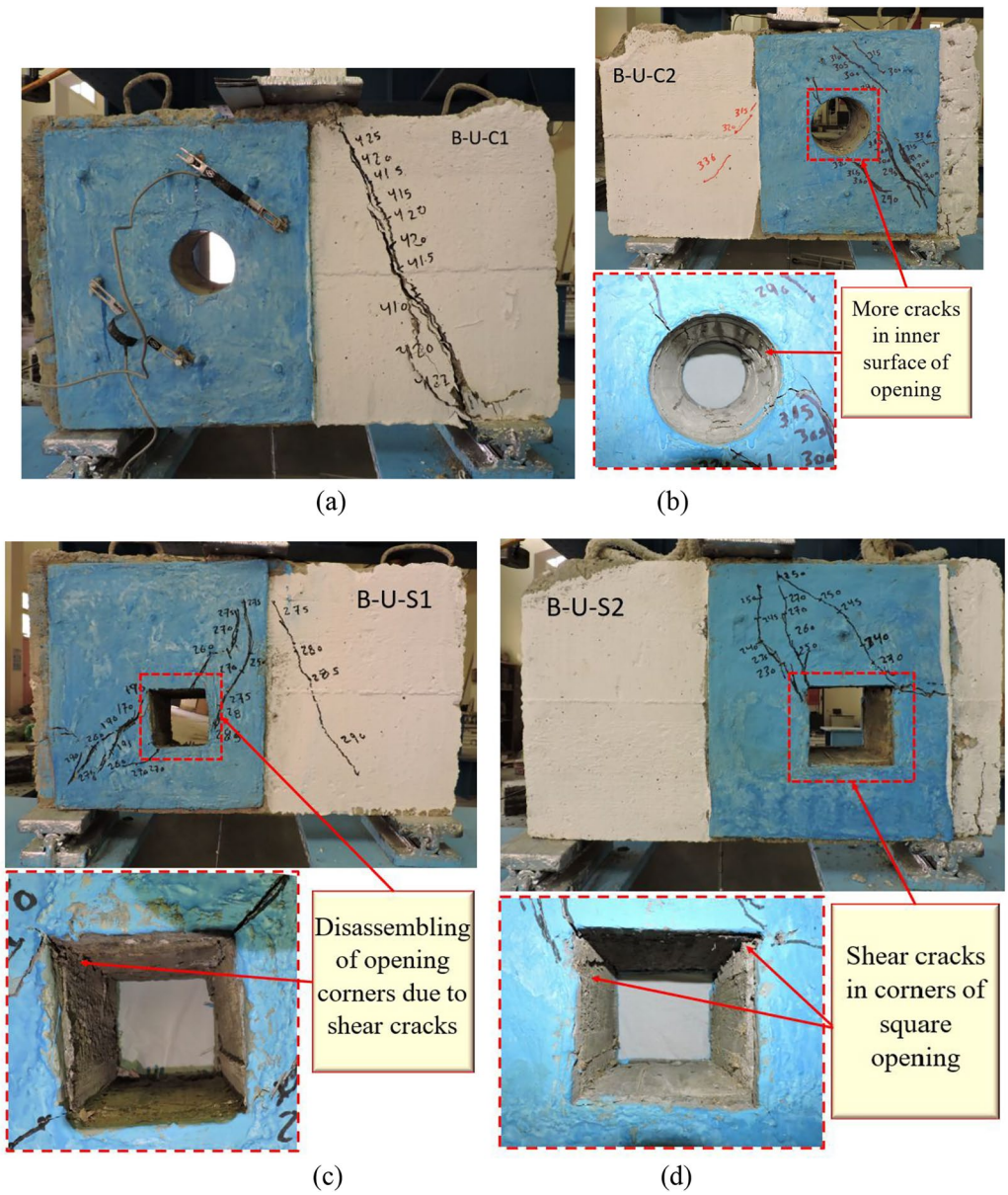

Fig. 10 Failure patterns of beams: **a** B-U-C1, **b** B-U-C2, **c** Bam B-U-S1, and **d** B-U-S2

This is because their geometry fosters a more favorable distribution of stress throughout the material than a square opening. Furthermore, circular openings influence crack patterns in a way that enhances the overall performance of the structure. Within the square opening beams (B-E-S1 and B-E-S2), smaller openings resulted in better behavior than larger ones. Notably, the beam with the larger square opening displayed behavior similar to but slightly better than the control beam throughout the loading stages. However, more improvement was observed for beams with smaller square openings. These findings suggest that the shape and size of openings significantly impact the behavior of beams under load.

Similar trends were observed in the group G3 utilizing the UHFRC layer. Beams with circular openings (B-U-C1 and B-U-C2) displayed significantly improved performance compared to B0. The cracking load of B-U-C1, and B-U-C2 increased by 28% and 19%, while their ultimate loads were a remarkable 52% and 38% higher than B0, respectively. However, beams with square openings (B-U-S1 and B-U-S2) exhibited a less pronounced improvement. Cracking load increased by 12% and 2%

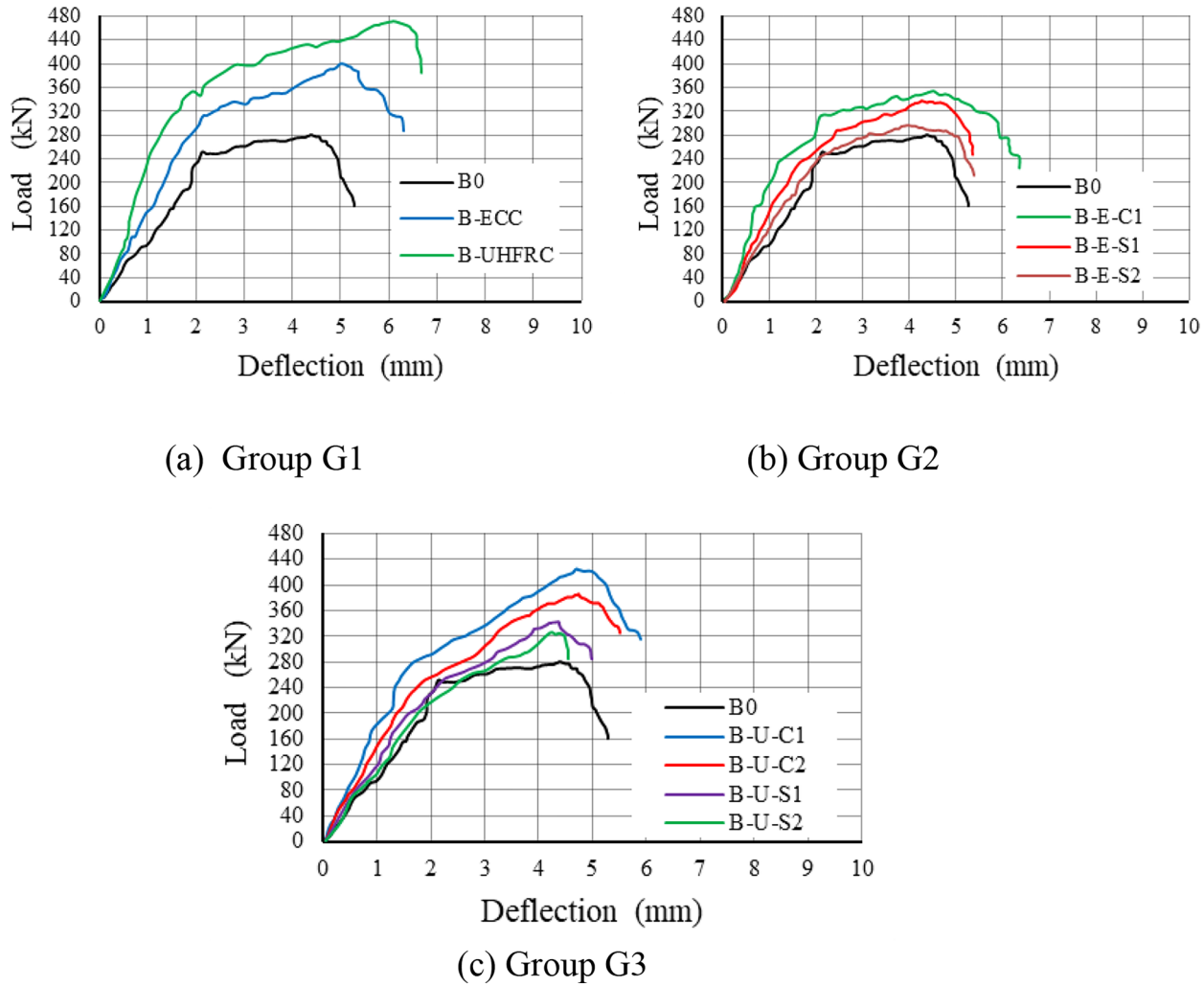

Fig. 11 Load–deflection curves of tested beams

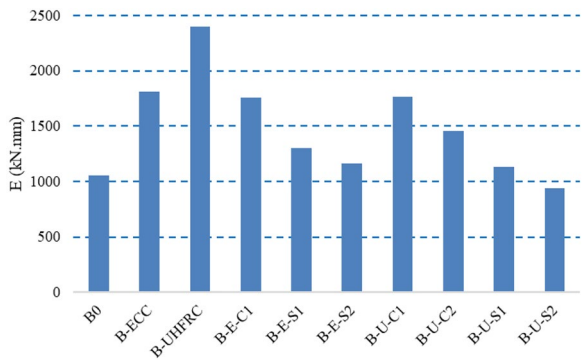

Fig. 12 Energy absorption of the beams (kN mm)

for B-U-S1 and B-U-S2, respectively, while ultimate load increased by 22% and 16%, respectively.

3.3 Absorbed Energy

The flexural energy absorption of the beams was calculated as the area under the measured load–deflection curves (Hamoda et al., 2024a, e, 2025). Fig. 12 presents the absorbed energy for all beams. Beams B-ECC and B-UHFRC in Gorup G1 exhibited an absorbed energy 72% and 127% greater than B0, respectively. Beam B-E-C1 in group G2, featuring a circular opening, demonstrated a remarkable 66% increase in the absorbed energy compared to the control beam. This increase was larger than the other two beams in this group featuring a square opening (B-E-S1, B-E-S2). As mentioned earlier, a circular opening fosters a more favorable distribution of stress than a square opening resulting in a higher energy absorption capacity. A similar pattern was observed for beams in group G3, where beams B-U-C1 and B-U-C2 exhibited a higher energy absorption capacity than beams B-U-S1 and B-U-S2. The increase of the absorbed energy

was calculated as 67% and 38% for B-U-C1 and B-U-C2, respectively, compared to B0, whereas the increase was calculated as only 7% for beam B-U-S1. A reduction of 12% of the energy absorption was observed for beam B-U-S2.

3.4 Elastic Stiffness

The elastic stiffness of the beams was calculated from the linear part of the load–deflection curves. Fig. 13 illustrates the elastic stiffness of the tested beams. It is observed that a substantial increase in the initial stiffness for beams in group G1, calculated as 35% and 97% for B-ECC and B-UHFRC compared to B0. This may be attributed to the superior characteristics of both ECC and UHFRC in the elastic performance allowing to exhibit high tensile ductility and tight crack width control. Moreover, the fibers help to bridge cracks and distribute stress more evenly, preventing the formation of large cracks and maintaining performance under load. For beams in group G2, Beam B-E-C1 in group G2, featuring a circular opening, demonstrated an 8% increase in stiffness compared to the control beam. The smaller increase may be expected to be due to the lower strength of the ECC. However, beams B-E-S1, and B-E-S2 exhibited an increase of 19%, and 10% compared to B0 which may reflect the effect of the opening size mentioned in Table 1. It is seen that increasing the opening size reduces the stiffness of the beam. When investigating the stiffness of the beams in group G3, it is seen that beams with circular openings (B-U-C1 and B-U-C2) had higher stiffness than their square counterparts. It may be because the stress distribution of stress in beams with circular openings was better than their square counterparts thus for the same strengthening technique, beams with circular openings outperform their square counterparts.

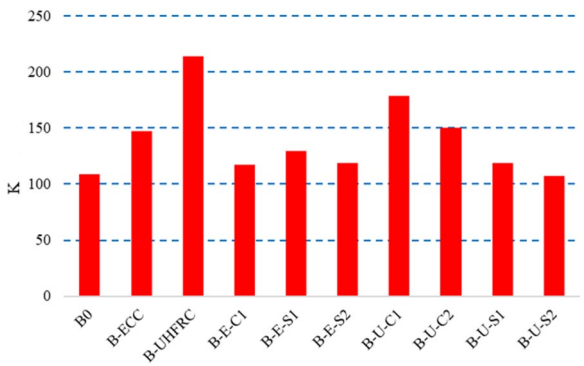

Fig. 13 Elastic stiffness for all beams. (Unit kN/mm)

4 FEM Simulation

4.1 Model Built-Up

To simulate the behavior of the deep RC beams tested, a finite element model (FEM) was developed using ABAQUS software (ABAQUS, 2009). Fig. 14 shows the model of a tested beam. In the modeling, the main beam, ECC/UHFRC layer, anchor bolts, and steel loading/support plates were modeled using solid elements (C3D8R) with reduced integration. Reinforcing rebars, stirrups, and WSM were represented by 3D truss elements (T3D2) to simulate their role in resisting both tension and compression forces.

The numerical study employed a detailed approach to simulate the interactions between various components of the strengthened beam. A surface-to-surface contact with a friction coefficient of 0.25 was used to model the interaction between the main concrete beam and the strengthening layer based on the sensitivity analysis. Reinforcing bars, stirrups were designed to be embedded in concrete and WSM was designed to be embedded in ECC/UHFRC layer. Finally, a perfect bond was assumed between the main beam and both the loading and supporting plates, signifying a rigid connection. The beam is hinged at the two bottom supports (Ux = Uy = UZ = Ury = Urz = 0), preventing any movement, while only rotation is allowed about *x*. The load is applied at the top middle point of the beam as a controlled displacement to simulate the loading process. The described boundary conditions were applied to reference points, which were connected to the loading and supporting plates using coupling constraints. This approach ensures the accurate transfer of forces and displacements between the reference points and the respective plates. The three-point loading setup was utilized for numerical study. This involved applying a displacement load along with specific boundary conditions to reference points associated with the steel plates using coupling constraints.

4.2 Materials Constitutive Modeling

To accurately capture the behavior of HSC, ECC, and UHFRC, the versatile Concrete Damage Plasticity (CDP) model was utilized (Hamoda et al., 2023a, 2024a, c). Accurate material laws are crucial for the model's validity. For HSC, the stress–strain relationship proposed by Carreira and Chu (1985) was implemented and calculated using Eqs. 1 and 2.

$$\sigma_c = f_c \left[\frac{\propto \left(\frac{\varepsilon_c}{\varepsilon_{c0}}\right)}{\propto -1 + \left(\frac{\varepsilon_c}{\varepsilon_{c0}}\right)^{\propto}} \right] \quad (1)$$

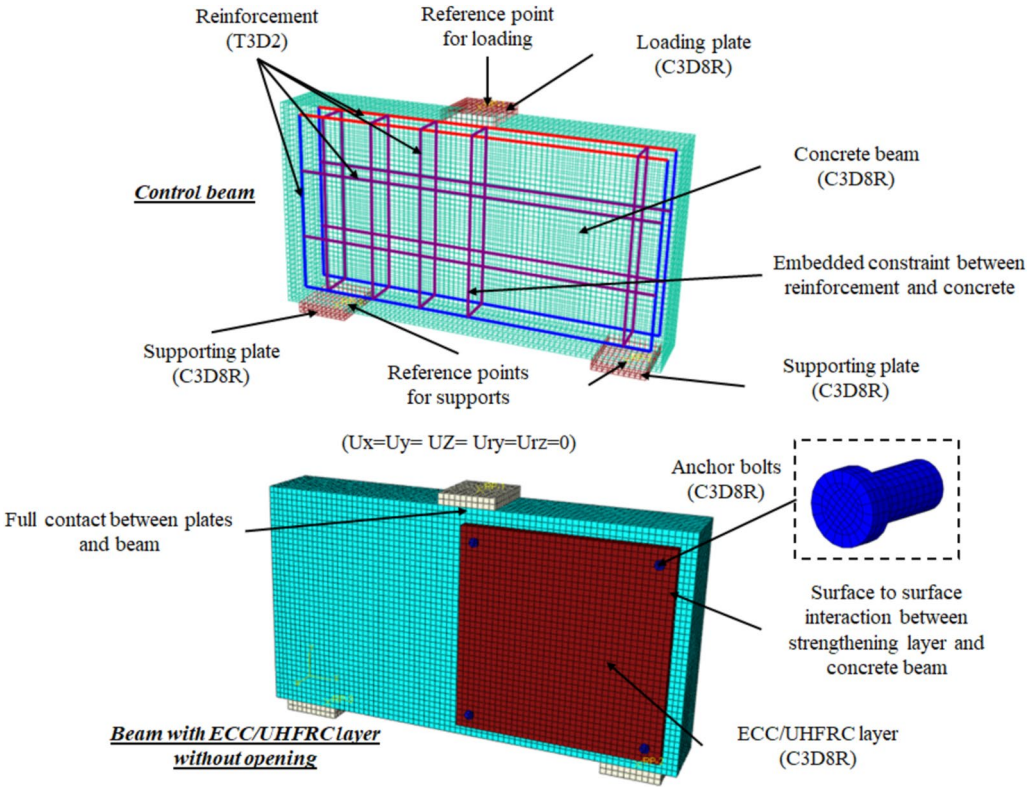

Fig. 14 Elements and contact of developed FEM

$$\sigma_t = \begin{cases} f_t \left[1.2\frac{\varepsilon_t}{\varepsilon_{t0}} - 0.2\left(\frac{\varepsilon_t}{\varepsilon_{t0}}\right)^6 \right] & 0 \le \varepsilon_t \le \varepsilon_{t0} \\ f_t \left[\frac{\frac{\varepsilon_c}{\varepsilon_0}}{1.25\left(\frac{\varepsilon_t}{\varepsilon_{t0}}-1\right)^2 - \frac{\varepsilon_t}{\varepsilon_{t0}}} \right] & \varepsilon_{t0} < \varepsilon_t \end{cases} \quad (2)$$

For ECC and UHFRC, previously established stress–strain correlations from Zhou et al. (2015) were adopted (Eqs. 3 and 4). Finally, a bi-linear elastic–plastic behavior model was utilized to represent the steel reinforcement within the concrete structures.

$$f_c = \begin{cases} E_0\, \varepsilon_c & \varepsilon_c \le 0.4\, \varepsilon_{cp} \\ E_0\, \varepsilon_c \left(1 - 0.308\frac{E_0\, \varepsilon_c}{f_c'} + 0.124\right) & 0.4\, \varepsilon_{cp} < \varepsilon_c \le \varepsilon_{cp} \end{cases} \quad (3)$$

$$f_t = \begin{cases} \frac{f_{tc}}{\varepsilon_{tc}}\varepsilon_t & 0 \le \varepsilon_t \le \varepsilon_{tc} \\ f_{tc} + \frac{f_{tu}-f_{tc}}{\varepsilon_{tu}-\varepsilon_{tc}}(\varepsilon - \varepsilon_{tc}) & \varepsilon_{tc} < \varepsilon_t \le \varepsilon_{tu} \end{cases} \quad (4)$$

The experimental stress–strain curve in this work was used to calculate the modulus of elasticity for each type of concrete directly. By capturing the distinct behavior of every type of concrete under stress, it guarantees a more realistic representation of the actual material characteristics used. The fitted/calibrated curves of concrete using the aforementioned formuals are shown in Fig. 3.

Based on the sensitivity analysis and previous recommendations, the adopted CDP parameters, namely, a ratio of second stress invariants of 0.66, a yield stress ratio of 1.16, and material-specific dilation angles (35° for ECC and UHFRC, maintaining the default 25° for HSC), a non-viscous material assumption ($\mu = 0.0$) and the default eccentricity ($e = 0.1$) (Hamoda et al., 2023b, d, e). The stress–strain curves of steel bars were idealized in straight lines as shown in Fig. 4 to reduce computational time. This is a common approach adopted by authors in their previous studies (Hamoda et al., 2024a, d, f). Furthermore, the research identified a mesh size of 10 mm as the optimal balance between computational efficiency and accuracy, significantly reducing simulation time. Modeling steel loading/support plates is important for loading and as mentioned earlier, they were modeled using solid elements (C3D8R) with reduced integration, having a mesh size of 10 mm.

4.3 FEM Validation

The accuracy of the developed finite element model is examined by comparing the predicted performance of deep beams with the test data including load–deflection curves (Fig. 15), failure modes (Fig. 16), and the load (see Table 5). The FEM effectively captured the entire

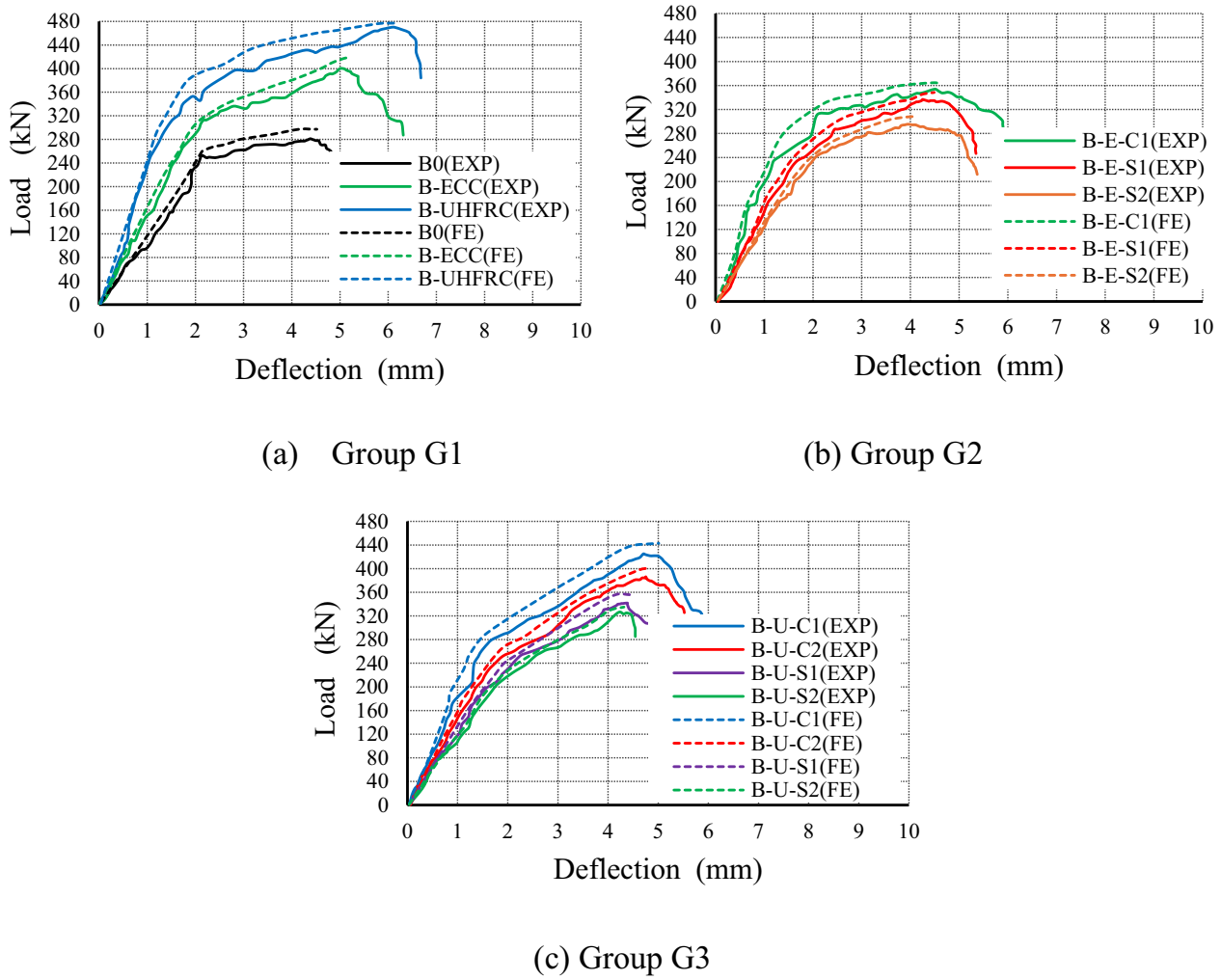

Fig. 15 Experimental and numerical load–deflection relationships for beams

load–deflection response of the beams, from the initial stages of cracking to the point of ultimate failure (see Fig. 15). The predictions are also very close to the test observation in terms of stiffness, ultimate load capacity, and deflection. Furthermore, the model successfully identified the different failure modes and crack patterns observed in the actual experiments (see Fig. 16). As shown in Fig. 16, the FEM predicted the pattern of the crack and it propagation towards the support as seen in the test for B0. When examining the failure modes of B-UHFRC, it is seen that the cracks are dense in the critical weak zones as seen in the test for beam B-UHFRC colored blue section. For beams B-E-C1 and B-U-S1, it is seen that the failure was due to the major cracks predicted through the opening as observed in the tests. It should be noted that, to assess the effectiveness of the proposed strengthening configuration in improving shear resistance, stirrups were strategically omitted from half of each beam. Thus failure of beams was predominated by the failure in one side of the beams.

In addition, the FEM results displayed excellent agreement with the experimental data when compared to the load (see Table 5). At the cracking and ultimate stage, the FEM's predictions for the loads were within 4% of the experimental values, with minimal variations across the test specimens. Similarly, when compared to the deflection at the cracking and ultimate stage, the model's predictions for both load and deflection closely matched the experimental results, with differences of 3% average calculated.

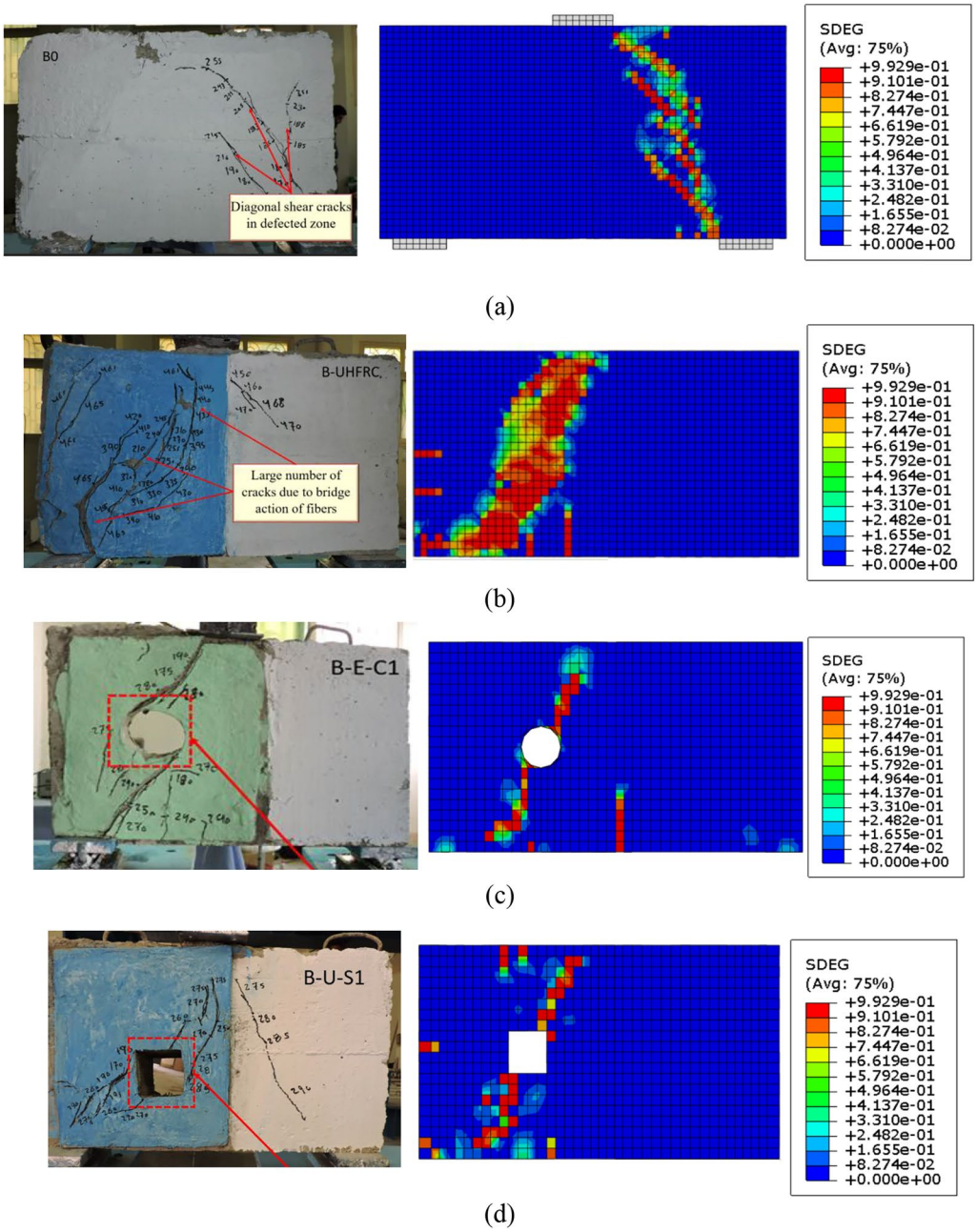

Fig. 16 Experimental and numerical crack patterns: **a** B0, **b** B-UHFRC, **c** B-E-C1, and **d** B-U-S1

5 Parametric Study

5.1 Effects of Thickness of ECC Layer

The validated FEM is carried out to study the effects of various thicknesses of the ECC layer on the ultimate capacity of the beams strengthened with HPC. Beam strengthened with circular opening, namely, specimen B-E-C1 tested in this study, was adopted for investigation. The details of the cross section and geometry were the same as the ones tested in this study. The thickness of the layer of ECC was varied from 10 to 25 mm in 1 mm increments resulting in the ratio of the thickness of the ECC layer to the thickness of the beam (t_{ECCC}/t_{beam}), which varied from 0.17 to 0.42. Fig. 17 illustrates the improvement of the ultimate strength due to the increase of the t_{ECCC}/t_{beam} ratio. It is seen that the ultimate strength of the beam increases as the t_{ECCC}/t_{beam} ratio increases. The increase of the ultimate strength of the beam was calculated as 22.6% when the t_{ECCC}/t_{beam}

Table 5 Comparisons of the test and FEM predictions

Specimen ID	P_{cr} (kN)			Δ_{cr} (mm)			P_u (kN)			Δ_{Pu} (mm)		
	EXP	FE	EXP/FE	EXP	FE	EXP/FE	EXP	FE	EXP/FE	EXP	FE	EXP/FE
B0	160	162	0.99	0.94	0.96	0.98	280.35	297.23	0.94	4.42	4.52	0.98
B-ECC	108.75	113.87	0.96	0.74	0.75	0.99	400.23	417.73	0.96	5.00	5.21	0.96
B-E-S1	102.20	106.11	0.96	0.79	0.82	0.96	336.77	348.53	0.97	4.25	4.48	0.95
B-E-S2	100.05	104.36	0.96	0.84	0.86	0.98	295.31	308.28	0.96	3.93	4.05	0.97
B-UHFRC	134.67	139.12	0.97	0.63	0.68	0.93	470.12	476.98	0.99	6.06	6.22	0.97
B-U-C2	121.43	126.83	0.96	0.81	0.84	0.96	386.25	399.35	0.97	4.75	4.84	0.98
B-U-S1	114.33	120.23	0.95	0.96	0.99	0.97	341.11	355.85	0.96	4.26	4.43	0.96
B-U-S2	104.20	110.41	0.94	0.97	1.01	0.96	325.16	335.05	0.97	4.37	4.40	0.99
Average (Avg)			0.96			0.97			0.96			0.97
Standard deviation (SD)			0.01			0.02			0.01			0.02
Coefficient of variation (COV)			0.001			0.002			0.001			0.002

FE Numerical prediction, *EXP* Test observation

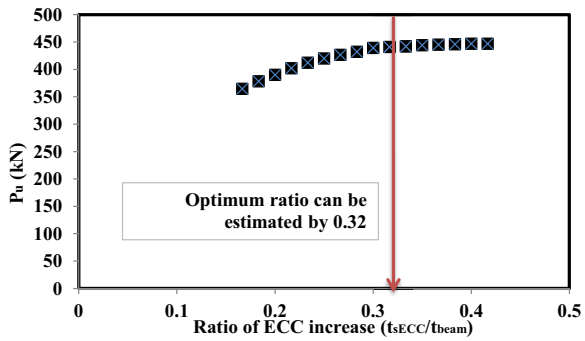

Fig. 17 Effects of the thickness of the ECC layer on the ultimate strength of the beam with circular openings strengthened using HPC

ratio increased from 0.17 to 0.42. However, one can see that the improvement of the ultimate strength becomes insignificant when the the t_{ECCC}/t_{beam} ratio exceeds 0.32. Thus, for practical design purposes, it is recommended that the the t_{ECCC}/t_{beam} ratio should not exceed 0.32 to achieve economic benefits.

5.2 Effects of Opening Ratio

To examine the effects of the size of the opening ratio, a beam strengthened with a square opening, namely, specimen B-U-S1 tested in this study was adopted for investigation. The size of the square opening varied from 85 × 85 to 200 × 200 mm, resulting in the opening-to-shear span

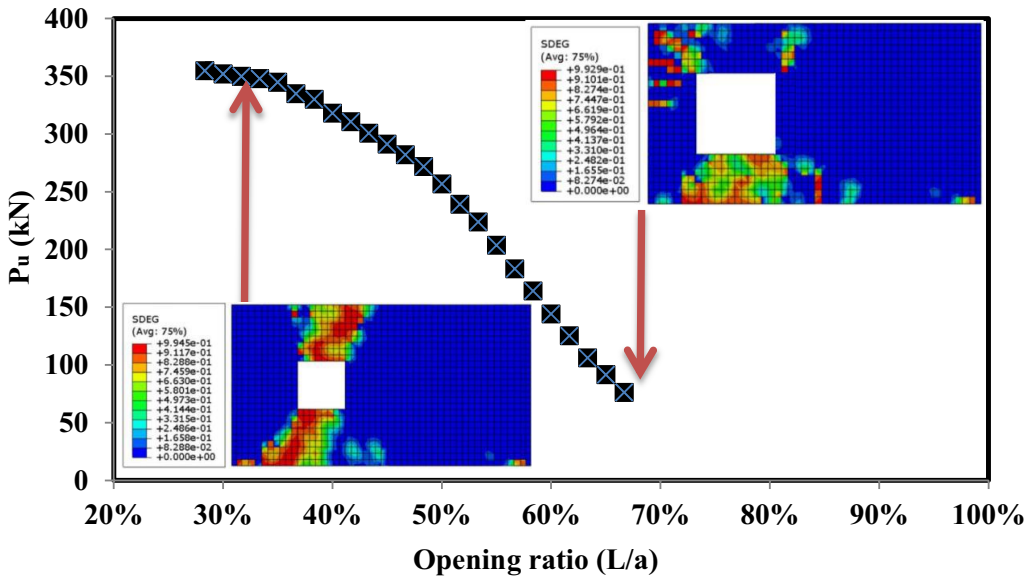

Fig. 18 Effects of the effects of the size of the opening ratio on the ultimate strength of the beam with square openings strengthened using HPC

(L/a) ratio varying from 28 to 67%, respectively. From the FEM results given in Fig. 18, it is seen that as the opening size increases, the ultimate load of the beams decreases significantly. However, initially, the rate of reduction is less significant as can be observed from Fig. 18. For instance, the reduction is only 7% for the increase of the L/a ratio from 28 to 38%. However, the reduction of the ultimate load is found to be significantly increased as the L/a ratio exceeds 38%. The ultimate load of the beams is found to be reduced by 78.5% when the L/a ratio varies from 28 to 67%. Increasing the L/a ratio significantly changes the failure modes of the beams as can be seen from Fig. 18.

6 Conclusions

This paper carries out experimental and numerical investigations on the performance of RC deep beams strengthened using externally bonded ECC/UHFRC layers reinforced with steel wire mesh. The key outcomes of this study can be listed as follows:

1. Strengthening of deep beams using ECC/UHFRC layers is found to improve the failure mode to a ductile mode compared to the control beam which failed due to brittle shear failure. The ultimate load of the tested strengthened beams was found to be increased in the range of 5–68% compared to the control beam.
2. The presence and size of openings in beams significantly influenced the performance of the beams. Bemas with circular openings outperformed the performance of beams with square openings. The increase of the load, energy absorption, and stiffness of the beams with circular openings for any kind of concrete was significantly higher than the beams with square openings.
3. Beams strengthened with UHFRC layers exhibited higher improvement in load, and stiffness compared to other beams cast with different concrete with or without an opening. For the identical beams with identical shapes and sizes of the opening, the application of UHFRC resulted in a significant improvement in their performance.
4. The parametric study shows that for the beams with circular openings strengthened with ECC layers, the improvement of the shear strength is negligible when t_{ECCC}/t_{beam} ratio exceeds 0.32. Furthermore, beams with square openings, the reduction of the ultimate load is found to be significantly increased as the opening-to-shear span (L/a) ratio exceeds 38%.

Abbreviations

a	Shear span
CDP	Concrete damage plasticity
ECC	Engineered CEMENTITIOUS COmposites
E	Absorbed energy
E_0	Stiffness of the concrete
e	Eccentricity
f'_c	Compressive strength
f_t	Tensile strength
f_c	Concrete's peak stress
f_{t0}	Concrete's tensile strength
f_{tu}	Tensile strength of the concrete
K	Elastic index
P_{cr}	Load corresponding to the first crack appeared
P_u	Ultimate load
UHFRC	Ultra-high-performance fiber-reinforced concrete
Δ_{cr}	Vertical deflection corresponding to P_{cr}
Δ_{Pu}	Vertical deflection corresponding to P_u
σ_c	Concrete longitudinal stress
ε_c	Strain corresponding to σ_c
ε_{co}	Strain at f_c
ε_{cp}	The strain of concrete at peak stress
α	Factor defined the specific shape of the concrete's stress–strain curve assumed to be 2.5 in this study
ε_{tc}	Strain at the first crack
ε_{tu}	Strain corresponding tensile strength
μ	Non-viscous material assumption for CDP model

Acknowledgements
Thanks to the technicians of the Concrete Structures Laboratory at Kafrelsheikh University in Egypt for their help.

Author contributions
Ahmed Hamoda: conceptualization, methodology, software, validation, formal analysis, investigation, data curation, writing–original draft, visualization, and project administration. Mohamed Emara: investigation, data curation, formal analysis, and writing–original draft. Mizan Ahmed: writing–original draft and visualization. Aref A. Abadel: visualization and writing–review and editing.

Funding
The authors would like to acknowledge the support provided by King Saud University in Riyadh, Saudi Arabia under project number RSP2025R343.

Availability of data and materials
The data sets used and/or analyzed during the current study are available from the corresponding author upon reasonable request.

Declarations

Competing interests
The authors declare that they have no competing interests.

Author details
[1]Civil Engineering Dept., Faculty of Engineering, Kafrelsheikh University, Kafrelsheikh, Egypt. [2]Structural Engineering Department, Faculty of Engineering, Zagazig University, Zagazig 44519, Egypt. [3]Centre for Infrastructure Monitoring and Protection, School of Civil and Mechanical Engineering, Curtin University, Kent Street, Bentley, WA 6102, Australia. [4]Department of Civil Engineering, College of Engineering, King Saud University, 11421 Riyadh, Saudi Arabia.

Received: 22 July 2024 Accepted: 11 January 2025
Published online: 19 August 2025

References

A370-10. (2006). *Standard test methods and definitions for mechanical testing of steel products*. ASTM International.

Abadel, A. A., Abbas, H., Almusallam, T., Alshaikh, I. M., Khawaji, M., Alghamdi, H., & Salah, A. A. (2022). Experimental study of shear behavior of CFRP strengthened ultra-high-performance fiber-reinforced concrete deep beams. *Case Studies in Construction Materials, 16*, e01103. https://doi.org/10.1016/j.cscm.2022.e01103

ABAQUS. (2009). *Abaqus user's manual version 69*. Dassault Systemes.

ACI 318-19. (2019). *Building code requirements for reinforced concrete*. American Concrete Institute.

Akkaya, H. C., Aydemir, C., & Arslan, G. (2022a). An experimental research on reinforced concrete deep beams fully wrapped with fiber reinforced polymers against shear. *Case Studies in Construction Materials, 17*, e01198. https://doi.org/10.1016/j.cscm.2022.e01198

Akkaya, H. C., Aydemir, C., & Arslan, G. (2022b). Investigation on shear behavior of reinforced concrete deep beams without shear reinforcement strengthened with fiber reinforced polymers. *Case Studies in Construction Materials, 17*, e01392. https://doi.org/10.1016/j.cscm.2022.e01392

Akkaya, H. C., Aydemir, C., & Arslan, G. (2024). Evaluation of shear behavior of short-span reinforced concrete deep beams strengthened with fiber reinforced polymer strips. *Engineering Structures, 299*, 117145.

Al-Enezi, M. S., Yousef, A. M., & Tahwia, A. M. (2023). Shear capacity of UHPFRC deep beams with web openings. *Case Studies in Construction Materials, 18*, e02105. https://doi.org/10.1016/j.cscm.2023.e02105

Al-khreisat, A., Abdel-Jaber, M. T., & Ashteyat, A. (2023). Shear strengthening and repairing of reinforced concrete deep beams damaged by heat using NSM-CFRP ropes. *Fibers, 11*(4), 35. https://doi.org/10.3390/fib11040035

Al-Mahbashi, M., Elsanadedy, H., Abbas, H., Abadel, A., & Al-Salloum, Y. (2023). Experimental and numerical study of high strength reinforced concrete continuous deep beams with circular and rectangular openings. *Journal of Building Engineering, 79*, 107868. https://doi.org/10.1016/j.jobe.2023.107868

Arabzadeh, A., & Karimizadeh, H. (2019). Experimental study of RC deep beams with opening and FRP composites installed by means of EBR and EBROG methods. *Construction and Building Materials, 208*, 780–791. https://doi.org/10.1016/j.conbuildmat.2019.03.055

Ary, M. I., & Kang, T.H.-K. (2012). Shear-strengthening of reinforced & pre-stressed concrete beams using FRP: Part I—review of previous research. *International Journal of Concrete Structures and Materials, 6*, 41–47. https://doi.org/10.1007/s40069-012-0004-1

ASTM C1583/C1583M-20. (2020M). *Standard test method for tensile strength of concrete surfaces and the bond strength or tensile strength of concrete repair and overlay materials by direct tension (pull-off method)*. American Society for Testing and Materials.

ASTM C469/C469M. (2022). *Standard test method for static modulus of elasticity and poisson's ratio of concrete in compression*. American Society for Testing and Materials.

Cakir, F., Aydin, M. R., Acar, V., Aksar, B., & Akkaya, H. C. (2023). An experimental study on RC beams shear-strengthened with intraply hybrid U-jackets composites monitored by digital image correlation (DIC). *Composite Structures, 323*, 117503.

Carreira, D. J., & Chu, K.-H. (1985). *Stress-strain relationship for plain concrete in compression*. Paper presented at the Journal Proceedings.

Chandrakanth, K., & Kavitha, P. (2020). *Shear strengthening of RC deep beam using steel plates*. Paper presented at the Proceedings of SECON'19: Structural engineering and construction management 3.

Choi, Y., Lee, H.-K., Chu, S., Cheong, S., & Jung, W. (2012). Shear behavior and performance of deep beams made with self-compacting concrete. *International Journal of Concrete Structures and Materials, 6*, 65–78. https://doi.org/10.1007/s40069-012-0007-y

Dutta, B., Kumari, A., & Nayak, A. N. (2022). Shear behaviour of RC deep beams retrofitted with externally bonded GFRP fabrics: Experimental and numerical study. *Structures, 46*, 1–16. https://doi.org/10.1016/j.istruc.2022.10.042

El Maaddawy, T., & Sherif, S. (2009). FRP composites for shear strengthening of reinforced concrete deep beams with openings. *Composite Structures, 89*(1), 60–69. https://doi.org/10.1016/j.compstruct.2008.06.022

Elsayed, M., Badawy, S., Tayeh, B. A., Elymany, M., Salem, M., & ElGawady, M. (2022). *Shear behaviour of ultra-high performance concrete beams with openings*. Paper presented at the Structures.

Emara, M., Salem, M. A., Mohamed, H. A., Shehab, H. A., & El-Zohairy, A. (2023). Shear strengthening of reinforced concrete beams using engineered cementitious composites and carbon fiber-reinforced polymer sheets. *Fibers, 11*(11), 98. https://doi.org/10.3390/fib11110098

Farouk, M. A., Moubarak, A. M., Ibrahim, A., & Elwardany, H. (2023). New alternative techniques for strengthening deep beams with circular and rectangular openings. *Case Studies in Construction Materials, 19*, e02288. https://doi.org/10.1016/j.cscm.2023.e02288

Fatehi Makki, R., Talib Jassem, A., & Abd Al-Latef Jassem, H. (2019). Behavior of reactive-powder concrete deep beams with CFRP-strengthened openings. *Practice Periodical on Structural Design and Construction, 24*(4), 04019016.

Ghali, M. K., Said, M., Mustafa, T., & El-Sayed, A. A. (2021). Behaviour of T-shaped RC deep beams with openings under different loading conditions. *Structures, 31*, 1106–1129. https://doi.org/10.1016/j.istruc.2021.01.091

Group, S. (2021). SikaFiber® PPM-12. Retrieved from https://gcc.sika.com/dms/getdocument.get/85409532-2a48-4092-b1b6-d89f05e9801f/sikafiber-ppm-12.pdf

Hamoda, A., Abadel, A. A., Ahmed, M., Wang, V., Vrcelj, Z., & Liang, Q. Q. (2025). Punching shear performance of reinforced concrete slab-to-steel column connections incorporating ECC and UHPECC. *Engineering Structures, 322*, 119145.

Hamoda, A., Abadel, A. A., Sennah, K., Ahmed, M., Zhang, X., & Emara, M. (2024a). Shear strengthening of RC beams incorporating post-tensioned bars and engineered cementitious composite reinforced with palm fronds. *Buildings, 14*(10), 3277.

Hamoda, A. A., Ahmed, M., Abadel, A. A., Ghalla, M., Patel, V. I., & Liang, Q. Q. (2023b). Experimental and numerical studies of circular precast concrete slender columns with intermediate connection filled with high-performance concrete. *Structures, 57*, 105204. https://doi.org/10.1016/j.istruc.2023.105204

Hamoda, A., Elsamak, G., Emara, M., Ahmed, M., & Liang, Q. Q. (2023a). Experimental and numerical studies of reinforced concrete beam-to-steel column composite joints subjected to torsional moment. *Engineering Structures, 275*, 115219. https://doi.org/10.1016/j.engstruct.2022.115219

Hamoda, A., Emara, M., Abadel, A. A., & Sennah, K. (2024b). Influence of shear strengthening of reinforced normal concrete beams incorporating sustainable materials. *Structural Concrete*. https://doi.org/10.1002/suco.202300556

Hamoda, A., Emara, M., Ahmed, M., Abadel, A. A., & Patel, V. I. (2024c). Flexural behavior of precast rectangular reinforced concrete beams with intermediate connection filled with high-performance concrete. *Buildings, 14*(9), 2823.

Hamoda, A., Ghalla, M., Yehia, S. A., Ahmed, M., Abadel, A. A., Baktheer, A., & Shahin, R. I. (2024d). Experimental and numerical investigations of the shear performance of reinforced concrete deep beams strengthened with hybrid SHCC-mesh. *Case Studies in Construction Materials, 21*, e03495.

Hamoda, A., Shahin, R. I., Ahmed, M., Abadel, A. A., Baktheer, A., & Yehia, S. A. (2024e). Strengthening of reinforced concrete columns incorporating different configurations of stainless-steel plates. *Structures, 64*, 106577.

Hamoda, A., Yehia, S. A., Ahmed, M., Abadel, A. A., Baktheer, A., & Shahin, R. I. (2024f). Experimental and numerical analysis of deep beams with openings strengthened with galvanized corrugated and flat steel sheets. *Case Studies in Construction Materials, 21*, e03522.

Heydari, P., Mostofinejad, D., Mostafaei, H., & Ahmadi, H. (2023). Strengthening of deep RC coupling beams with FRP composites: A numerical study. *Structures, 51*, 435–454. https://doi.org/10.1016/j.istruc.2023.03.071

Jasim, W. A., Tahnat, Y. B. A., & Halahla, A. M. (2020). Behavior of reinforced concrete deep beam with web openings strengthened with (CFRP) sheet. *Structures, 26*, 785–800. https://doi.org/10.1016/j.istruc.2020.05.003

Kachouh, N., El-Maaddawy, T., El-Hassan, H., & El-Ariss, B. (2022). Shear response of recycled aggregates concrete deep beams containing steel fibers and web openings. *Sustainability, 14*(2), 945. https://doi.org/10.3390/su14020945

Koutas, L. N., Tetta, Z., Bournas, D. A., & Triantafillou, T. C. (2019). Strengthening of concrete structures with textile reinforced mortars: State-of-the-art

review. *Journal of Composites for Construction, 23*(1), 03118001. https://doi.org/10.1061/(ASCE)CC.1943-5614.0000882
Kumari, A., & Nayak, A. (2021). Strengthening of shear deficient RC deep beams using GFRP sheets and mechanical anchors. *Canadian Journal of Civil Engineering, 48*(1), 1–15. https://doi.org/10.1139/cjce-2019-0333
Lee, H.-K., Cheong, S., Ha, S.-K., & Lee, C. (2011). Behavior and performance of RC T-section deep beams externally strengthened in shear with CFRP sheets. *Composite Structures, 93*(2), 911–922. https://doi.org/10.1016/j.compstruct.2010.07.002
Li, R., Deng, M., Zhang, Y., & Wei, D. (2022). Shear strengthening of reinforced concrete deep beams with highly ductile fiber-reinforced concrete jacket. *Journal of Building Engineering, 48*, 103957. https://doi.org/10.1016/j.jobe.2021.103957
Nakamura, H., Iwamoto, T., Fu, L., Yamamoto, Y., Miura, T., & Gedik, Y. H. (2018). Shear resistance mechanism evaluation of RC beams based on arch and beam actions. *Journal of Advanced Concrete Technology, 16*(11), 563–576. https://doi.org/10.3151/jact.16.563
Osman, B. H., Wu, E., Ji, B., & Abdulhameed, S. S. (2017). Repair of pre-cracked reinforced concrete (RC) Beams with openings strengthened using FRP sheets under sustained load. *International Journal of Concrete Structures and Materials, 11*, 171–183. https://doi.org/10.1007/s40069-016-0182-3
Rahim, N. I., Mohammed, B. S., Al-Fakih, A., Wahab, M., Liew, M., Anwar, A., & Amran, Y. M. (2020). Strengthening the structural behavior of web openings in RC deep beam using CFRP. *Materials, 13*(12), 2804. https://doi.org/10.3390/ma13122804
Shakir, Q. M., & Alghazali, A. F. (2024). Effect of the arching action on the behavior of the RC precast concrete deep beams: Comparison between several hybrid models. *Journal of Building Pathology and Rehabilitation, 9*(1), 23. https://doi.org/10.1007/s41024-023-00377-0
Shakir, Q. M., Al-Sahlawi, Y. M., Abd, B. B., & Hamad, S. A. (2023). Nonlinear finite element analysis of high-strength reinforced concrete beams with severely disturbed regions. *Jordan Journal of Civil Engineering, 17*(1), 23–33.
Shakir, Q. M., & Hamad, S. H. (2023). Reinforced Concrete Beams with Drop-in-Ends of Vertical and Inclined Reinforcement and having Pockets Loaded by In-Plane Static Forces. *Journal of Materials and Engineering Structures, 10*(1), 33–49.
Shakir, Q. M., & Hannon, H. K. (2024). Innovative model of precast RC curved hybrid deep beams composed partially with high-performance concrete. *Arabian Journal for Science and Engineering, 49*(4), 6045–6060.
Shakir, Q. M., & Hanoon, H. K. (2023). New models for reinforced concrete precast hybrid deep beams under static loads with curved hybridization. *Structures, 54*, 1007–1025.
Shakir, Q. M., & Yahya, Y. M. (2024). Stitching of T-deep beams with large openings by CFRP sheets and NSM steel bars. *Pollack Periodica*.
Shyamala, G. (2022). Impact of reinforcement and geometry of deep beam–Research perspective. *Materials Today: Proceedings, 68*, 1556–1561. https://doi.org/10.1016/j.matpr.2022.07.189
Sika Egypt. Retrieved from https://egy.sika.com/en/construction/concrete-repair/concrete-repair-system/epoxy-base-repairsytems/epoxy-repair-mortars/sikadur-31-cf-slow.html
Wang, G., Yang, C., Pan, Y., Zhu, F., Jin, K., Li, K., & Nanni, A. (2019). Shear behaviors of RC beams externally strengthened with engineered cementitious composite layers. *Materials, 12*(13), 2163. https://doi.org/10.3390/ma12132163
Xing, Z., Zhu, Y., Shao, Y., Ma, E., Chung, K.-F., & Chen, Y. (2024). Experimental and numerical research on shear performance of GFRP bar reinforced seawater sea-sand concrete deep beams without stirrups. *Case Studies in Construction Materials, 20*, e03142. https://doi.org/10.1016/j.cscm.2024.e03142
Yousef, A. M., Tahwia, A. M., & Al-Enezi, M. S. (2023). Experimental and numerical study of UHPFRC continuous deep beams with openings. *Buildings, 13*(7), 1723.
Yousef, A. M., Tahwia, A. M., & Marami, N. A. (2018). Minimum shear reinforcement for ultra-high performance fiber reinforced concrete deep beams. *Construction and Building Materials, 184*, 177–185.
Zhou, J., Pan, J., & Leung, C. K. (2015). Mechanical behavior of fiber-reinforced engineered cementitious composites in uniaxial compression. *Journal of Materials in Civil Engineering, 27*(1), 04014111. https://doi.org/10.1061/(ASCE)MT.1943-5533.0001034

Publisher's Note

Ahmed Hamoda Assistant Professor, Civil Engineering Dept., Faculty of Engineering, Kafrelsheikh University, Kafrelsheikh, Egypt

Mohamed Emara Associate Professor, Structural Engineering Department, Faculty of Engineering, Zagazig University, Zagazig, 44,519, Egypt

Mizan Ahmed Lecturer, Centre for Infrastructure Monitoring and Protection, School of Civil and Mechanical Engineering, Curtin University, Kent Street, Bentley, WA 6102, Australia

Aref A. Abadel Associate Professor, Department of Civil Engineering, College of Engineering, King Saud University, Riyadh 11,421, Saudi Arabia